

# Comparing electron-phonon coupling strength in diamond, silicon and silicon carbide: First-principles study

Bartomeu Monserrat\* and R. J. Needs

*TCM Group, Cavendish Laboratory, University of Cambridge,  
J. J. Thomson Avenue, Cambridge CB3 0HE, United Kingdom*

(Dated: August 20, 2018)

Renormalization of the electronic band gap due to electron-phonon coupling in the tetrahedral semiconductors diamond, silicon and cubic silicon carbide is studied from first principles. There is a marked difference between the coupling of the vibrational state to the valence band maximum and to the conduction band minimum. The strength of phonon coupling to the valence band maximum is similar between the three systems and is dominated by vibrations that change the bond length. The coupling strength to the conduction band minimum differs significantly in diamond, silicon carbide and silicon. In diamond, the coupling is dominated by six small pockets of vibrational states in the phonon Brillouin zone, that are ultimately responsible for the stronger electron-phonon coupling in this material. Our results represent a first step towards the development of an *a priori* understanding of electron-phonon coupling in semiconductors and insulators, that should aid the design of materials with tailored electron-phonon coupling properties.

## I. INTRODUCTION

Electron-phonon coupling is ubiquitous in condensed matter physics. It plays a central role in mediating the attractive interaction between electrons within the BCS theory of conventional superconductivity,<sup>1,2</sup> and it leads to the temperature dependence of electronic energy levels.<sup>3</sup> Technological applications driven by these effects include high-field magnets,<sup>4</sup> photovoltaics, and light emitting diodes.

The theoretical study of electron-phonon coupling in semiconductors was established by the pioneering work of Allen, Heine, and Cardona.<sup>5,6</sup> Recently, their ideas have been applied using accurate first-principles density functional theory (DFT) methods.<sup>7-10</sup> DFT calculations not only give accurate predictions of the temperature dependence of band gaps, but also allow us to investigate the underlying microscopic physics.

The strength of electron-phonon coupling in semiconductors can be gauged by the size of the correction to the band gap from the zero-point (ZP) nuclear motion. Experiments have focused on the effects of the isotopic mass  $m$ ,<sup>3,11-13</sup> and, as the amplitude of the atomic vibrations scales as  $m^{-1/2}$ , a heavier isotope leads to weaker electron-phonon coupling. This explanation is related to the qualitative considerations of Han and Bester<sup>14</sup>, who compare the ZP gap correction for a range of semiconductors, and find that the magnitude of the correction is very roughly proportional to the ratio  $\sqrt{\langle u^2 \rangle}/a$ , where  $\sqrt{\langle u^2 \rangle}$  is the mean atomic ZP displacement, and  $a$  is the lattice parameter. Electronic effects are considered by Cardona<sup>13</sup>, who argues that, as first row atoms (like carbon) have no core  $p$  electrons, the valence electrons are strongly influenced by atomic vibrations, leading to stronger electron-phonon coupling compared to systems with core  $p$  electrons (like silicon).

In this work we present a first-principles study of the strength of electron-phonon coupling in the tetrahedrally

bonded semiconductors diamond (C), cubic silicon carbide (SiC), and silicon (Si). These systems have the same crystal structure, and similar electronic band structures and phonon dispersions. However, the effects of electron-phonon coupling are significantly different between them, and therefore they represent an interesting set of test systems. Our approach allows us to disentangle the vibrational and electronic contributions and to evaluate their relative importance. A complex picture emerges with different behaviour of the coupling of the valence band minimum (VBM) and the conduction band maximum (CBM) to the vibrational state. The electron-phonon coupling strength for the VBM is similar in the three systems and dominated by vibrations that change the bond length between nearest neighbour atoms. The coupling strength for the CBM varies significantly and in a non-trivial manner across the three systems studied, and accounts for the majority of the difference in the coupling strengths of C, SiC, and Si. We find strong coupling in C which arises from the vibrational states in six small pockets in the phonon Brillouin zone (BZ).

This work represents a step towards a quantitative understanding of the various factors influencing electron-phonon coupling in semiconductors. This understanding could ultimately lead to the development of strategies for designing new materials with tailored electron-phonon coupling properties, a topic of great interest for many technological applications.<sup>15</sup>

The paper is arranged as follows. In Sec. II we describe the theoretical and computational methods used for calculating electronic and vibrational properties, and their coupling. In Sec. III we present our results for the various contributions to the electron-phonon coupling strength in C, SiC, and Si, and we summarize our findings in Sec. IV. All equations are given in Hartree atomic units, in which the Dirac constant, the electronic charge and mass, and  $4\pi$  times the permittivity of free space are unity ( $\hbar = |e| = m_e = 4\pi\epsilon_0 = 1$ ).

## II. THEORETICAL AND COMPUTATIONAL FRAMEWORKS

### A. Structural parameters

We have studied C, SiC, and Si in their tetrahedrally bonded diamond structures within plane-wave pseudopotential DFT<sup>16,17</sup> as implemented in the CASTEP package.<sup>18</sup> We have used the local density approximation (LDA)<sup>19,20</sup> functional and ultrasoft pseudopotentials<sup>21</sup> for C and Si. All energy differences between the different frozen phonon configurations used for the electron-phonon coupling calculations are converged to better than  $10^{-4}$  eV per unit cell, requiring a plane-wave energy cut-off of 800 eV, and a Monkhorst-Pack<sup>22</sup> BZ sampling grid of density  $2\pi \times 0.03 \text{ \AA}^{-1}$ .

We have relaxed the structures until the force on each atom is smaller than  $10^{-4}$  eV/Å and the components of the stress tensor are less than  $10^{-2}$  GPa. This leads to the lattice constants shown in Table I, which are in good agreement with experiment, and are used throughout. The LDA functional tends to overbind because it favours uniform charge densities, as shown in Table I.

### B. Electronic structure

The electronic configuration of C is  $1s^2 2s^2 2p^2$ , and when it forms diamond the  $2s$  and  $2p$  electrons hybridize to form four  $sp^3$  orbitals which give rise to the tetrahedrally bonded structure. The electronic configuration of Si is  $1s^2 2s^2 2p^6 3s^2 3p^2$  and a similar hybridization occurs, but with the  $3s$  and  $3p$  electrons. The valence electrons in Si are farther away from the nucleus, which has been invoked to explain the weaker electron-phonon coupling in Si compared to diamond.<sup>13</sup>

In Fig. 1 we show the electronic band structures of C, Si, and SiC along symmetry lines, and densities of electronic states. The band structures are similar, with the VBM located at the  $\Gamma$ -point and the CBM located along the symmetry line between  $\Gamma$  and X.

### C. Phonon dispersion

We have constructed the matrix of force constants from the forces on the atoms calculated with finite atomic displacements of magnitude  $0.005 \text{ \AA}$ , averaging over positive

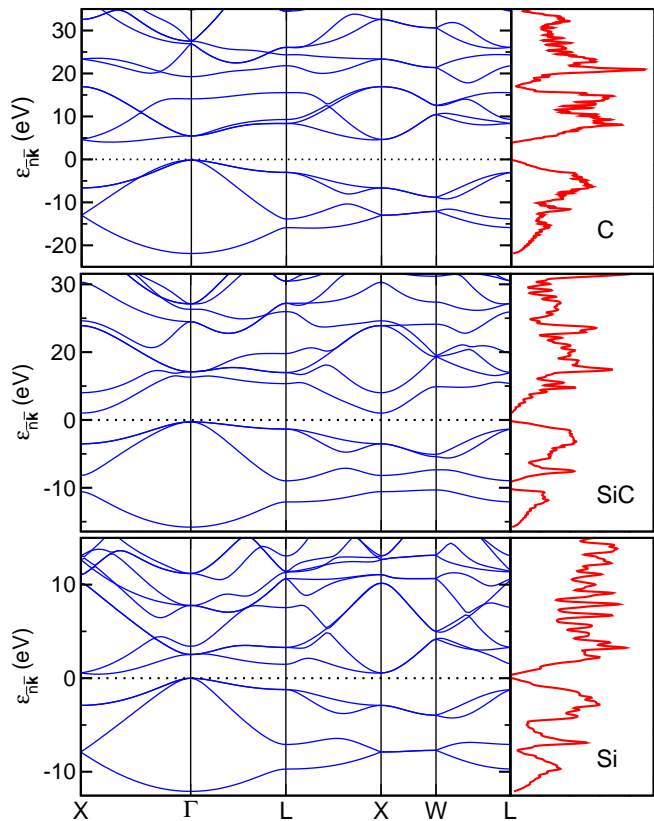


FIG. 1. (color online) Electronic band structures along symmetry lines of the first electron BZ (blue, left side), and electronic densities of states (red, right side) of C, SiC, and Si. The dotted line shows the VBM. The wave vector axes have been scaled so that each plot has the same width.

and negative displacements.<sup>26</sup> We have then diagonalized the dynamical matrix for the points along symmetry lines of the first phonon BZ. Points in the phonon BZ are labelled by  $\mathbf{k}$ , and branches by  $n$ . The force constants decay in real space as a function of atomic separation, and we have found that for all three systems  $5 \times 5 \times 5$  supercells containing 250 atoms leads to converged results for the vibrational energy.

In Fig. 2 we show the phonon dispersions and densities of states of C, Si, and SiC. Considering SiC as an example, we have found that the highest energy phonon branch corresponds to vibrations dominated by the motion of C atoms. The two other optical branches correspond to antiphase vibrations of neighbouring Si and C atoms. The highest energy acoustic branch is dominated by the motion of Si atoms, and the two lowest energy branches correspond to long wave length vibrations. We note that the optical branches of SiC are subject to LO-TO splitting, calculated using density functional perturbation theory as implemented in the CASTEP code.<sup>27</sup>

The ZP energies per primitive unit cell of C, SiC, and Si are given in Table II. As expected, the lighter materials have larger ZP energies. The ZP energies are converged to within  $10^{-4}$  eV per primitive unit cell with respect to

TABLE I. Static LDA-DFT and experimental lattice parameters of C, SiC, and Si in the diamond structure.

	$a_{\text{theor,static}} (\text{\AA})$	$a_{\text{exp}} (\text{\AA})$
C	3.529	3.567 <sup>23</sup>
SiC	4.318	4.3581 <sup>24</sup>
Si	5.394	5.4298 <sup>25</sup>

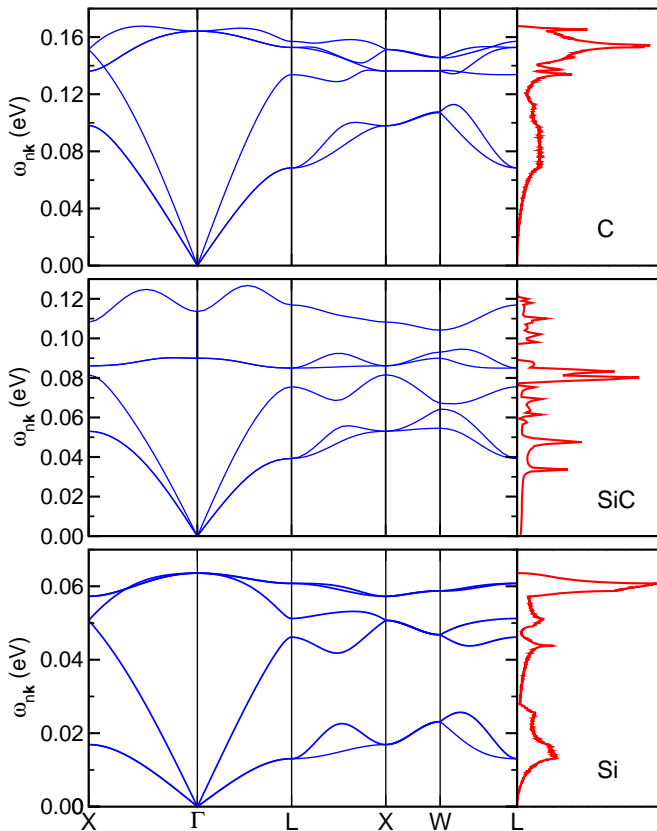


FIG. 2. (color online) Phonon dispersions along symmetry lines of the first phonon BZ (blue, left side), and phonon densities of states (red, right side) of C, SiC, and Si. The wave vectors axes have been scaled so that each plot has the same width.

the size of the supercell.

#### D. Electron-phonon coupling

The effect of electron-phonon coupling on the band gap of a semiconductor can be calculated by considering the change in the vibrational free energy arising from the promotion of an electron from the valence to the conduction band,<sup>7</sup> or by calculating the change in the electronic bands due to the presence of vibrations.<sup>5,6</sup> These two approaches can be shown to be equivalent, at least in lowest order perturbation theory.<sup>28</sup>

TABLE II. Vibrational ZP energy per primitive unit cell of C, SiC, and Si in the diamond structure at the theoretical equilibrium volumes.

	ZP energy (eV)
C	0.368
SiC	0.223
Si	0.123

We use the second approach and calculate the zero temperature electron-phonon correction to the electronic thermal (minimum) band gap  $E_g$  as

$$\langle E_g \rangle = \langle \Phi(\mathbf{q}) | E_g(\mathbf{q}) | \Phi(\mathbf{q}) \rangle, \quad (1)$$

where  $|\Phi\rangle$  is the ground state vibrational wave function. We work within the harmonic approximation, and therefore the vibrational wave function  $|\Phi\rangle$  is a Hartree product of simple harmonic oscillator eigenstates for each vibrational mode, which are simple Gaussian functions for the ground state.

The expression in Eq. (1) has been evaluated in the literature by sampling  $E_g$  using path integral methods<sup>29,30</sup> or Monte Carlo methods,<sup>31,32</sup> or by using some variant of the expansion<sup>9,14,33</sup>

$$E_g(\mathbf{q}) = \sum_{n,\mathbf{k}} a_{n\mathbf{k}} q_{n\mathbf{k}}^2, \quad (2)$$

where  $q_{n\mathbf{k}}$  is the amplitude of the vibrational mode labeled by  $(n, \mathbf{k})$ . Evaluating Eq. (1) using the approximate expression of Eq. (2) is similar to using the Allen-Heine-Cardona theory, but the expression in Eq. (2) is more accurate because it includes the so-called non-diagonal Debye-Waller term that is missing in the Allen-Heine-Cardona theory.<sup>34</sup> We note that it excludes terms with higher powers of  $q_{n\mathbf{k}}$  and coupling between different points in the BZ, whereas sampling methods include all of these terms and should therefore be more accurate. However, this expansion allows us to investigate the contribution from each vibrational mode independently, which is obscured in a sampling approach, and furthermore, the expansion in Eq. (2) has been found to lead to very good agreement with experiment for a range of materials, including diamond.<sup>8,9</sup> Our calculations of the ZP corrections to the band gaps of C, SiC, and Si are shown in Table III and compared with experimental estimates of ZP band gap corrections where available.<sup>35</sup> The experimental estimate of  $-0.364$  eV for C is obtained from isotopic data in Ref. 13, and the estimate of  $-0.410$  eV from an extension of the typical Bose-Einstein oscillator fit to the temperature dependence of the band gap in Ref. 33. In this work we calculate band gap corrections using Eq. (2).

The strategy we follow in Sec. III is to evaluate the couplings  $a_{n\mathbf{k}}$  for each vibrational mode labelled by  $(n, \mathbf{k})$ . This allows us to determine which vibrational modes contribute to the overall electron-phonon correction to the band gap. We work within the Born-Oppenheimer approximation, which implies that the couplings  $a_{n\mathbf{k}}$  are independent of temperature. Therefore, without loss of generality, we focus on the ZP correction to the band gap.

We use the harmonic wave functions obtained as described in Sec. II C and calculate the couplings  $a_{n\mathbf{k}}$  by performing frozen-phonon calculations for the  $\mathbf{k}$ -points in the irreducible phonon BZ. The frozen phonon calcu-

lation for the vibrational mode labelled by  $(n, \mathbf{k})$  is performed at a vibrational amplitude of magnitude about  $\sqrt{\langle q_{n\mathbf{k}}^2 \rangle}$ , and we have averaged over positive and negative displacements. Our results are for supercells constructed from  $6 \times 6 \times 6$  primitive unit cells in the case of C, and from  $5 \times 5 \times 5$  primitive unit cells for SiC and Si, unless otherwise stated. The ZP band gap correction for C converges slowly with respect to the size of the supercell (see Table III). This is a well-known feature in C,<sup>10</sup> and the slow convergence with respect to phonon BZ sampling will prove to be intimately related to the electron-phonon coupling strength in C, as discussed in Sec. III C.

We also note that the use of DFT for calculating electron-phonon induced band gap corrections is appropriate, although LDA-DFT is not accurate for the calculation of the absolute value of band gaps. The usual band gap underestimation of standard DFT approximations affects all frozen-phonon configurations in a very similar manner, and therefore it is expected to cancel in the calculation of the band gap correction as it is the difference between the static band gap  $E_g$  and the renormalized band gap  $\langle E_g \rangle$ . This is supported by the numerical results of Giustino and co-workers in Ref. 8.

### III. RESULTS

The ZP band gap correction for C is several hundreds of meVs, while in Si it is about 6 times smaller. In this section we investigate the underlying microscopic properties that give rise to the ZP band gap corrections.

#### A. Microscopic description of the strength of electron-phonon coupling

In Fig. 3 we show the electron-phonon contribution  $\Delta\epsilon(\omega)$  to the band gap correction as a function of the harmonic vibrational mode frequency  $\omega$  for C, SiC, and Si. These results correspond to a supercell containing 432 atoms (1296 vibrational modes) for C, and 250 atoms (750 vibrational modes) for SiC and Si, which is equivalent to a phonon BZ sampling using  $6 \times 6 \times 6$  and  $5 \times 5 \times 5$

TABLE III. ZP band gap corrections for C, SiC, and Si as a function of supercell size. Experimental results are also shown where available.

BZ grid	C	SiC	Si
$3 \times 3 \times 3$	-0.401 eV	-0.110 eV	-0.053 eV
$4 \times 4 \times 4$	-0.292 eV	-0.089 eV	-0.052 eV
$5 \times 5 \times 5$	-0.325 eV	-0.109 eV	-0.060 eV
$6 \times 6 \times 6$	-0.334 eV		
Exp.	-0.364 eV <sup>13</sup>		-0.053 eV <sup>13</sup>
	-0.410 eV <sup>33</sup>		

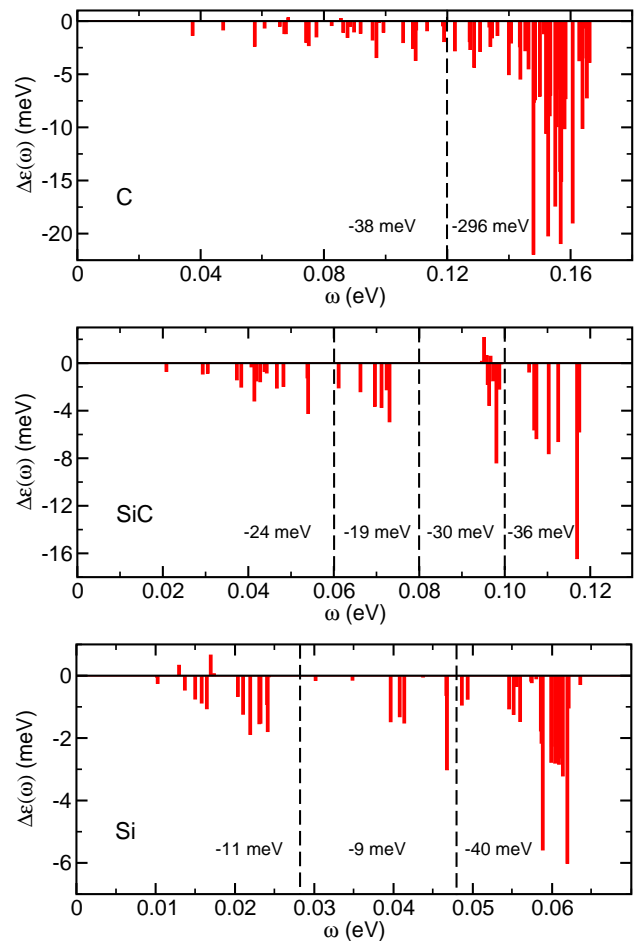


FIG. 3. (color online) ZP band gap corrections  $\Delta\epsilon(\omega)$  as a function of the frequency  $\omega$  of the vibrational modes for C, SiC, and Si. The vertical dashed lines separate intervals of the phonon branches with different vibrational characters (see text for details). The numbers reported for each of these intervals correspond to the integrated correction to the band gap for that interval.

grids, respectively.

For C, the phonon density of states (see Fig. 2) can be divided into low- and high-energy branches, with a division at about 0.12 eV. The high-energy branches correspond to vibrational modes in which nearest-neighbour atoms vibrate out of phase. For SiC, as discussed in Sec. II C, the vibrational modes can be divided into the motion of C atoms, optical vibrations, the motion of Si atoms, and acoustic vibrations. These divisions correspond to energies of 0.06 eV, 0.08 eV, and 0.10 eV. In the case of Si, we have divided the vibrational modes into three classes delimited by energies of 0.028 eV and 0.048 eV. These divisions are shown as vertical dashed lines in Fig. 3. In each case we have integrated the electron-phonon contribution to the change in the gap for the specified vibrational frequency intervals  $(\omega_1, \omega_2)$  as  $\int_{\omega_1}^{\omega_2} \Delta\epsilon(\omega) d\omega$ , which are also given in Fig. 3.

In all three systems the dominant contribution to the

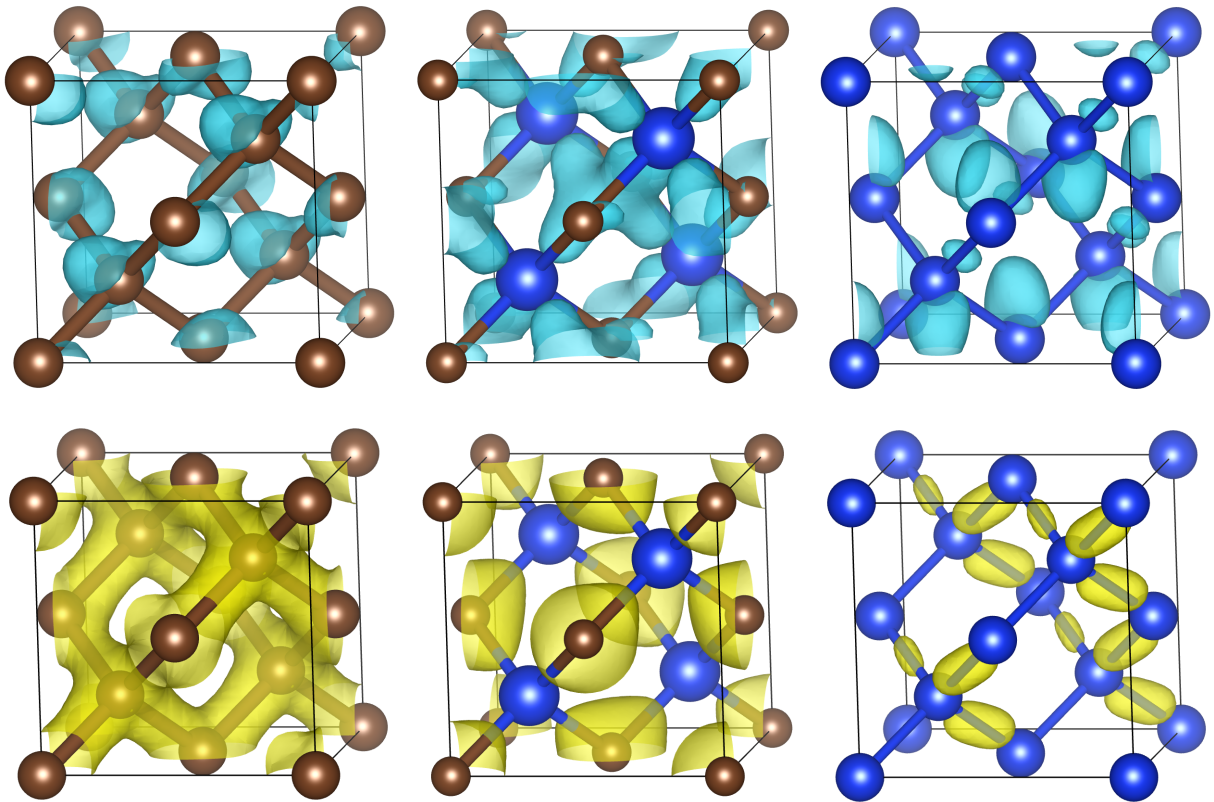


FIG. 4. (color online) Charge density isosurfaces of the electronic state corresponding to the CBM (top three) and VBM (bottom three) for diamond (left), silicon carbide (center), and silicon (right). The structures are not to scale.

correction to the band gap arises from the highest energy vibrational modes, which correspond to optical phonons. In C the correction due to the optical modes clearly dominates, but for SiC and Si the low energy modes make an important contribution as well.

### B. Valence band maximum

In the bottom row of Fig. 4 we show the charge density of the VBM for C, SiC, and Si, which is concentrated around the bonds for C and Si. SiC is an ionic material, and the valence charge density is therefore attracted towards the more electronegative C nuclei, although still oriented along the bond direction. The electronic charge density along the bonds is shown in the upper diagram of Fig. 5. The location of the charge density agrees with the observation from Fig. 3 that in each material the dominant contribution to the band gap correction arises from optical modes, as these vibrations change the length of the interatomic bonds in which the charge density associated with the VBM resides.

The ZP band gap correction of C and Si over the phonon BZ is shown in Fig. 6 in the 2-dimensional slice defined by  $\mathbf{c}^* = \mathbf{0}$ . The vectors  $(\mathbf{a}^*, \mathbf{b}^*, \mathbf{c}^*)$  are the reciprocal lattice vectors. The vibrations that couple strongly

to the VBM charge density by changing the bond length form a shell around the  $\Gamma$ -point in the phonon BZ, indicated in Fig. 6 by the red solid circles.

The lower diagram of Fig. 5 demonstrates that the average charge density  $\rho$  along the bond obeys  $\rho \propto a^{-1}$ , where  $a$  is the lattice parameter. This simple dependence of the charge density associated with the VBM, together with the very similar coupling to the VBM between C and Si shown in Fig. 6, cannot explain the strong non-linearity found by Han and Bester in the band gap correction as a function of lattice parameter  $a$ .<sup>14</sup>

### C. Conduction band minimum

The top row of Fig. 4 also shows the charge density of the CBM for C, SiC, and Si. The charge density is localized around the atomic sites, in contrast to the bond localized charge density of the VBM.

Two major features can be seen in the ZP band gap correction for C over the phonon BZ shown in Fig. 6. The first is the shell around the  $\Gamma$ -point (red solid circle), that is a consequence of the coupling of optical-like vibrations that change the bond lengths and couple strongly with the charge density associated with the VBM as discussed above. This feature is present in both C and Si,

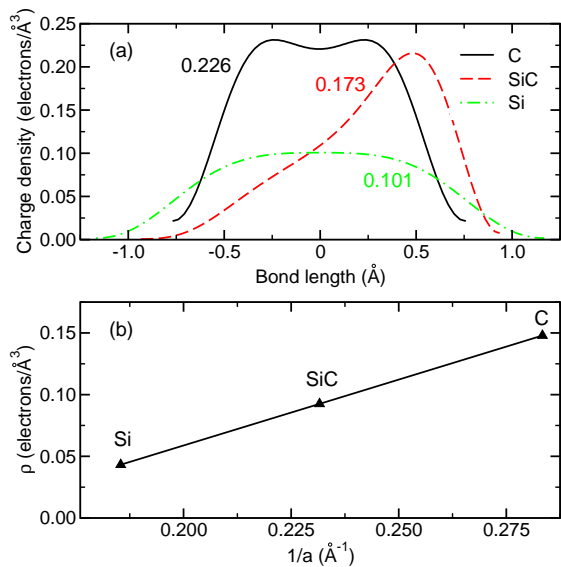


FIG. 5. (color online) (a) Charge density of the electronic state corresponding to the VBM along a bond of C (solid black line), SiC (dashed red line), and Si (dashed-dotted green line). In each case we also give the integrated charge density along the bonds, averaged over the four bonds of the tetrahedral structure. For SiC, the C atom is at the right of the figure, where the charge density is larger. (b) The average bond density  $\rho$  as a function of the inverse lattice constant  $a^{-1}$ .

as the VBM charge density is very similar between these systems. However, in C (and only in C), there is a further strong variation, indicated by blue dashed circles in Fig. 6. This second strong variation in C is dominated by modes in the neighbourhood of the reciprocal space point  $(\mathbf{a}^*/3, -\mathbf{b}^*/3, 0)$  and symmetry-related points in the phonon BZ, where the ZP correction to the band gap is large. There are a total of six such spherical-like pockets in the phonon BZ, of which we show a cross-section of two in Fig. 6.

The charge density corresponding to the bottom of the conduction bands of C, SiC, and Si is antibonding. When the structures are distorted along vibrational modes, the charge density changes in such a way as to preserve the antibonding nature. For the mode at the reciprocal space point  $(\mathbf{a}^*/3, -\mathbf{b}^*/3, 0)$ , the charge density in C is distorted significantly from the equilibrium charge density, whereas the corresponding distortion in Si is smaller. The vibrational mode has a wavelength of 3 primitive unit cells, and the local tetrahedral structure around a particular C atom is modified such that one bond remains at its equilibrium length, one (or two) bonds lengthen, and two (or one) bonds shorten. The charge density is then distorted so that it is concentrated along the directions of the longer bonds, as would be expected of an antibonding state (see Fig. 7). In Si, the charge density responds in a similar manner, but the changes are much smaller, leading to significantly weaker electron-phonon coupling than in C.

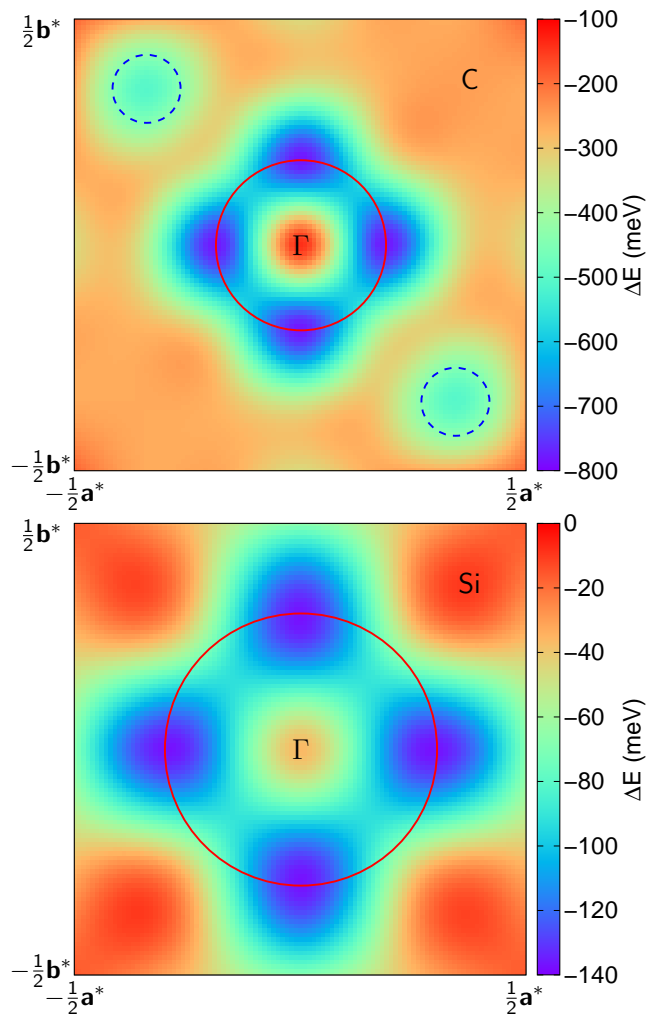


FIG. 6. (color online) ZP correction to the band gap of C and Si over 2-dimensional slices of the phonon BZ defined by  $\mathbf{c}^* = \mathbf{0}$ . For each  $\mathbf{k}$ -point we have summed over the six phonon branches present. The red solid circles indicate the region of strong electron-phonon coupling of the VBM, and the dashed blue circles indicate the region of strong coupling to the CBM. The overall ZP correction to the band gap is  $-334$  meV for C and  $-60$  meV for Si.

It is worth pointing out that it is also this difference between C and Si that leads to the slower convergence of the band gap correction of C with the density of BZ sampling (see Table III).

In order to investigate the origin of the difference in responses of the charge densities of C and Si, we consider the correction to the band gap due to electron-phonon coupling as a function of lattice parameter. The changes in lattice constant shown in Fig. 8 are equivalent to the application of an external isotropic compression (favoring smaller lattice constants) or dilation (favoring a larger lattice constant). These calculations use a supercell containing  $3 \times 3 \times 3$  primitive unit cells and 54 atoms, which is sufficient for our purposes, as the  $3 \times 3 \times 3$  supercell leads to converged results for Si, and includes the points

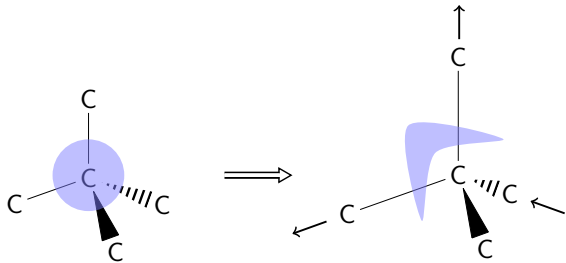


FIG. 7. (color online) Schematic of the bond distortion in the C tetrahedra for the vibration at the reciprocal-space point  $(\mathbf{a}^*/3, -\mathbf{b}^*/3, \mathbf{0})$  in the phonon BZ. The charge density (blue) accumulates near the two stretched bonds due to its antibonding nature.

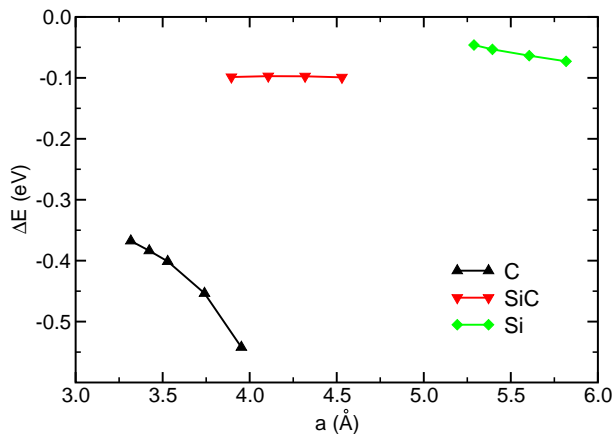


FIG. 8. (color online) ZP band gap correction for C (black up triangles), SiC (red down triangles), and Si (green diamonds) as a function of lattice parameter  $a$ . The solid lines are a guide to the eye.

in the phonon BZ of diamond that couple strongly to the electronic CBM (see Fig. 6). The electron-phonon coupling strength in C increases with lattice constant  $a$ . This increase is dominated by the six pockets in the phonon BZ that correspond to coupling to the CBM, and that are still located around the point  $(\mathbf{a}^*/3, -\mathbf{b}^*/3, \mathbf{0})$ , and correspond to similar atomic displacements for the structures at different  $a$ . The stronger coupling with increasing  $a$  can be understood by a complementary increase in  $\sqrt{\langle u^2 \rangle}$  for the modes dominating the coupling, which means that  $\sqrt{\langle u^2 \rangle}/a$  is an increasing function of  $a$ . Therefore, the ratio  $\sqrt{\langle u^2 \rangle}/a$  plays an important role in the strength of electron-phonon coupling within C. The different responses of C and Si are caused by the shorter bond lengths in C, where the atomic displacements represent a larger fraction of the bond length, and induce a stronger charge distortion to preserve the antibonding nature of the CBM.

It is interesting to note that the results shown in Fig. 8 have implications for the electron-phonon coupling correction to the band gap of C as a function of temperature. Increasing temperature leads to thermal expansion,

which increases the lattice parameter  $a$ . The strong dependence of the band gap correction on  $a$  in C suggests that a study of the temperature dependence of the band gap should include calculations of the correction as a function of volume.

## D. Discussion

The strength of electron-phonon coupling as reflected by the ZP correction to the VBM is similar in the three tetrahedral semiconductors considered. This emerges from the coupling of the optical vibrational modes to the VBM charge density, which is localized along the bonds.

In contrast, the picture for the ZP correction to the CBM is more complex. In all three systems, for a given vibrational amplitude the charge density distorts in order to preserve the antibonding nature of the CBM, but while this distortion is moderate in SiC and Si, it is very strong for C, especially in some regions of the phonon BZ. This is related to the larger value of the ratio  $\sqrt{\langle u^2 \rangle}/a$  in C compared to SiC and Si.

It is useful to reconsider earlier work in view of our findings. The arguments put forward previously in order to explain the difference in electron-phonon coupling strength between C and Si can be classified as vibrational arguments and electronic arguments:

(1) *Vibrational arguments.* Han and Bester<sup>14</sup> observe in a range of semiconductors that the electron-phonon coupling strength is an increasing function of  $\sqrt{\langle u^2 \rangle}/a$ , albeit in a very non-linear fashion. We have found that this non-linearity arises from the different vibrational couplings to the CBM in the three systems, which has a much larger amplitude in C for the modes around six localized pockets of the phonon BZ. These vibrational modes lead to very strong electron-phonon coupling. This suggests that the non-linear behaviour observed by Han and Bester is dominated by the coupling of the CBM to the vibrational states of the system.

(2) *Electronic arguments.* Cardona<sup>13</sup> has argued that the different strengths of electron-phonon coupling in C and Si are due to the presence of core  $p$ -states in Si that screen the atomic potential from the valence electrons more effectively than in C. However, the charge densities of the VBM and CBM differ significantly from atomic densities, and it is the distortion of the bonds rather than the motion of the nuclei with respect to an atomic-like charge density that drives electron-phonon coupling. It is interesting to note that the larger charge density in the bonds of C is due to the denser structure of C. The core  $p$  states in Si therefore *indirectly* reduce the strength of electron-phonon coupling, but by making Si less dense than C, rather than by directly affecting the distortions of the charge density via vibrations.

The core  $p$  states of Si in SiC lead to localization of the charge density along the bonds near the carbon atoms (see the top diagram of Fig. 5). However, this is due to the presence of *both* carbon and silicon atoms.

In Fig. 3 we observe that the vibrational modes dominated by carbon motion (correction of  $-36$  meV, for  $\omega > 0.10$  eV) lead to a larger correction to the band gap than those dominated by the motion of silicon (correction of  $-19$  meV, for  $0.06 < \omega < 0.08$  eV). However, if we renormalize the carbon motion value to take into account the enhancement of the vibrational motion of carbon atoms due to their smaller mass, we find  $\sqrt{m_C/m_{Si}} \times (-36) = \sqrt{12/28} \times (-36) = -24$  meV, which is only slightly larger than the silicon-motion-dominated correction ( $-19$  meV), and is not enough to explain the difference in strength between the ZP band gap corrections of C and Si. Furthermore, the marginal difference is due to the charge density being more strongly localized near the carbon atom in the bond, but this only arises because *both* carbon and silicon are present, and it would not occur in pure C or Si. This discussion suggests that the simple electronic argument of Cardona<sup>13</sup> cannot account for the different electron-phonon coupling strengths in C and Si.

#### IV. CONCLUSIONS

We have investigated electronic and vibrational properties of C, SiC, and Si using first principles DFT calculations. We have discussed the electron-phonon coupling induced correction of the electronic thermal band gaps of these semiconductors, focusing on the underlying microscopic properties. This has allowed us to disentangle the various contributions to the band gap corrections arising from coupling between the vibrations and electronic states. We have found very different behaviour in the coupling of the vibrational state to the VBM and CBM. The ZP correction to the VBM can be described in a similar manner for all three systems. In contrast, for the

CBM there are marked differences between C and Si/SiC, with the stronger coupling in C arising from a small number of vibrational modes in six small quasi-spherical pockets in the phonon BZ. This stronger coupling arises from the larger ratio  $\sqrt{\langle u^2 \rangle}/a$  in C. The stronger coupling of the CBM to the vibrational motion in C is responsible for the overall larger band gap correction than in Si/SiC.

This is, as far as we are aware, the first quantitative investigation of the underlying processes which determine the strength of electron-phonon coupling in semiconductors. Our results for C, SiC, and Si should not be extended to other types of semiconducting materials without careful consideration, as they might show different behaviour. Similar studies of other classes of semiconductors could increase our understanding of the relative importance of the contributions to electron-phonon coupling in systems with a band gap, and this knowledge could prove valuable in the design of new materials with tailored properties.

Finally, we note that a similar approach could be taken to investigate the underlying microscopic properties of the coupling between the vibrational state of a solid and physical quantities other than the electronic band gap.

#### ACKNOWLEDGMENTS

We thank Michael Rutter for implementing the calculation of the charge density along a line in the CHECK2XSF program. Financial support was provided by the Engineering and Physical Sciences Research Council (UK). The calculations were performed on the Cambridge High Performance Computing Service facility and the ARCHER UK National Supercomputing Service (<http://www.archer.ac.uk>), for which access was obtained via the UKCP consortium, EP/K013564/1.

- 
- \* [bm418@cam.ac.uk](mailto:bm418@cam.ac.uk)
- <sup>1</sup> L. N. Cooper, *Phys. Rev.* **104**, 1189 (1956).
  - <sup>2</sup> J. Bardeen, L. N. Cooper, and J. R. Schrieffer, *Phys. Rev.* **106**, 162 (1957).
  - <sup>3</sup> M. Cardona and M. L. W. Thewalt, *Rev. Mod. Phys.* **77**, 1173 (2005).
  - <sup>4</sup> J. E. Kunzler, E. Buehler, F. S. L. Hsu, and J. H. Wernick, *Phys. Rev. Lett.* **6**, 89 (1961).
  - <sup>5</sup> P. B. Allen and V. Heine, *J. Phys. C* **9**, 2305 (1976).
  - <sup>6</sup> P. B. Allen and M. Cardona, *Phys. Rev. B* **23**, 1495 (1981).
  - <sup>7</sup> R. D. King-Smith, R. J. Needs, V. Heine, and M. J. Hodgeson, *Europhys. Lett.* **10**, 569 (1989).
  - <sup>8</sup> F. Giustino, S. G. Louie, and M. L. Cohen, *Phys. Rev. Lett.* **105**, 265501 (2010).
  - <sup>9</sup> B. Monserrat, N. D. Drummond, and R. J. Needs, *Phys. Rev. B* **87**, 144302 (2013).
  - <sup>10</sup> S. Ponc e, G. Antonius, P. Boulanger, E. Cannuccia, A. Marini, M. C ot e, and X. Gonze, *Comput. Mater. Sci.* **83**, 341 (2014).
  - <sup>11</sup> A. T. Collins, S. C. Lawson, G. Davies, and H. Kanda, *Phys. Rev. Lett.* **65**, 891 (1990).
  - <sup>12</sup> C. Parks, A. K. Ramdas, S. Rodriguez, K. M. Itoh, and E. E. Haller, *Phys. Rev. B* **49**, 14244 (1994).
  - <sup>13</sup> M. Cardona, *Solid State Commun.* **133**, 3 (2005).
  - <sup>14</sup> P. Han and G. Bester, *Phys. Rev. B* **88**, 165311 (2013).
  - <sup>15</sup> A. Benyamini, A. Hamo, S. V. Kusminskiy, F. von Oppen, and S. Ilani, *Nat. Phys.* **10**, 151 (2014).
  - <sup>16</sup> P. Hohenberg and W. Kohn, *Phys. Rev.* **136**, B864 (1964).
  - <sup>17</sup> W. Kohn and L. J. Sham, *Phys. Rev.* **140**, A1133 (1965).
  - <sup>18</sup> S. J. Clark, M. D. Segall, C. J. Pickard, P. J. Hasnip, M. I. J. Probert, K. Refson, and M. C. Payne, *Z. Kristallogr.* **220**, 567 (2005).
  - <sup>19</sup> D. M. Ceperley and B. J. Alder, *Phys. Rev. Lett.* **45**, 566 (1980).
  - <sup>20</sup> J. P. Perdew and A. Zunger, *Phys. Rev. B* **23**, 5048 (1981).
  - <sup>21</sup> D. Vanderbilt, *Phys. Rev. B* **41**, 7892 (1990).
  - <sup>22</sup> H. J. Monkhorst and J. D. Pack, *Phys. Rev. B* **13**, 5188 (1976).
  - <sup>23</sup> H. Judith Grenville-Wells and K. Lonsdale, *Nature* **181**, 758 (1958).



- <sup>24</sup> J.-M. Bind, *Mater. Res. Bull.* **13**, 91 (1978).
- <sup>25</sup> D. N. Batchelder and R. O. Simmons, *J. Chem. Phys.* **41**, 2324 (1964).
- <sup>26</sup> K. Kunc and R. M. Martin, *Phys. Rev. Lett.* **48**, 406 (1982).
- <sup>27</sup> K. Refson, P. R. Tulip, and S. J. Clark, *Phys. Rev. B* **73**, 155114 (2006).
- <sup>28</sup> P. Allen and J. Hui, *Z. Phys. B* **37**, 33 (1980).
- <sup>29</sup> R. Ramírez, C. P. Herrero, and E. R. Hernández, *Phys. Rev. B* **73**, 245202 (2006).
- <sup>30</sup> M. A. Morales, J. M. McMahon, C. Pierleoni, and D. M. Ceperley, *Phys. Rev. B* **87**, 184107 (2013).
- <sup>31</sup> C. E. Patrick and F. Giustino, *Nat. Commun.* **4**, 2006 (2013).
- <sup>32</sup> B. Monserrat, N. D. Drummond, C. J. Pickard, and R. J. Needs, *Phys. Rev. Lett.* **112**, 055504 (2014).
- <sup>33</sup> B. Monserrat, G. J. Conduit, and R. J. Needs, [arxiv:1308.3483](https://arxiv.org/abs/1308.3483) (2013).
- <sup>34</sup> X. Gonze, P. Boulanger, and M. Côté, *Ann. Phys.* **523**, 168 (2011).
- <sup>35</sup> In Ref. 9 we reported a ZP band gap correction for diamond of  $-0.462$  eV. Those calculations used a  $3 \times 3 \times 3$  supercell, and should therefore be compared with the value of  $-0.401$  eV reported in Table III. The difference between these two values is due to the different treatment of the vibrational wave function and  $E_g(\mathbf{q})$ . In Ref. 9, we used an anharmonic vibrational wave function and a principal axes expansion for  $E_g(\mathbf{q})$ .